INTERNATIONAL JOURNAL FOR NUMERICAL METHODS IN FLUIDS
Int. J. Numer. Meth. Fluids 2008; **57**:177–204
Published online 16 October 2007 in Wiley InterScience (www.interscience.wiley.com). DOI: 10.1002/fld.1631

Finite-volume multi-stage schemes for shallow-water flow simulations

Wen-Dar Guo[1], Jihn-Sung Lai[1,*,†] and Gwo-Fong Lin[2]

[1]*Hydrotech Research Institute, National Taiwan University, Taipei 10617, Taiwan*
[2]*Department of Civil Engineering, National Taiwan University, Taipei 10617, Taiwan*

SUMMARY

A finite-volume multi-stage (FMUSTA) scheme is proposed for simulating the free-surface shallow-water flows with the hydraulic shocks. On the basis of the multi-stage (MUSTA) method, the original Riemann problem is transformed to an independent MUSTA mesh. The local Lax–Friedrichs scheme is then adopted for solving the solution of the Riemann problem at the cell interface on the MUSTA mesh. The resulting first-order monotonic FMUSTA scheme, which does not require the use of the eigenstructure and the special treatment of entropy fixes, has the generality as well as simplicity. In order to achieve the high-resolution property, the monotonic upstream schemes for conservation laws (MUSCL) method are used. For modeling shallow-water flows with source terms, the surface gradient method (SGM) is adopted. The proposed schemes are verified using the simulations of six shallow-water problems, including the 1D idealized dam breaking, the steady transcritical flow over a hump, the 2D oblique hydraulic jump, the circular dam breaking and two dam-break experiments. The simulated results by the proposed schemes are in satisfactory agreement with the exact solutions and experimental data. It is demonstrated that the proposed FMUSTA schemes have superior overall numerical accuracy among the schemes tested such as the commonly adopted Roe and HLL schemes. Copyright © 2007 John Wiley & Sons, Ltd.

Received 23 May 2007; Revised 3 September 2007; Accepted 4 September 2007

KEY WORDS: shallow-water flows; hydraulic shocks; multi-stage method; Riemann problem; local Lax–Friedrichs scheme; surface gradient method

1. INTRODUCTION

Free-surface shallow-water flows with hydraulic shock waves are commonly modeled by the two-dimensional (2D) shallow-water equations (SWE), which are considered as a non-linear system of hyperbolic conservation laws. Various types of monotonic numerical schemes developed for solving hyperbolic systems of conservation laws have been proposed in the literature [1–6]. These

*Correspondence to: Jihn-Sung Lai, Hydrotech Research Institute, National Taiwan University, Taipei 10617, Taiwan.
†E-mail: jslai525@ntu.edu.tw

Contract/grant sponsor: National Science Council, Taiwan; contract/grant numbers: NSC 95-2625-Z-002-022, NSC 95-2622-E-002-011-CC3

schemes require the well-known monotonic numerical fluxes for resolving discontinuities without spurious oscillations [4–6].

In general, there are two main approaches for establishing a monotonic numerical flux [5]. A simplest approach uses a centred or symmetric stencil and does not explicitly employ wave-propagation information. This approach results in the so-called centred schemes, such as the Lax–Friedrichs scheme and the first-order centred (FORCE) scheme [5]. The more accurate approach adopts the wave-propagation viewpoint in the solution of the Riemann problem and leads to the so-called upwind schemes or Riemann solvers [6]. The Riemann problem can be exactly solved. However, the expensive iterative procedures are required for the exact Riemann solver [5]. Thus, the so-called approximate Riemann solvers are more efficient and become practically popular for the constructions of the numerical fluxes, such as the Roe scheme [1], the Steger–Warming splitting (SWS) scheme [2], the Osher scheme [3], the Harten, Lax and van Leer (HLL) scheme [5], etc.

In recent years, many monotonic centred or upwind schemes have been applied to the simulations of shallow-water flows *via* the finite-volume method (FVM). For instance, Zoppou and Roberts [7] employed the HLLC scheme, where C stands for contact, for modeling the dam-break problems. Toro [8] presented the Lax–Friedrichs scheme and the FORCE scheme for the dam-break flow simulations. Wan *et al*. [9] adopted the Osher scheme to the practical flow simulation in the natural-irregular river topography. Erduran *et al*. [10] presented the performance tests of the five monotonic upwind schemes, namely the Osher, the HLL, the HLLC, the Roe and the SWS schemes. They found that the SWS scheme is the most efficient and the Osher scheme is the most accurate among the schemes tested. Lai *et al*. [11] proposed a robust and efficient hybrid flux-splitting finite-volume (HFF) scheme for simulating hydraulic shock waves. Lately, Lai *et al*. [12] proposed an upstream flux-splitting finite-volume (UFF) scheme for the solutions of the 2D SWE. The UFF scheme was also compared with the commonly used Osher, Roe and HLL schemes. The UFF scheme has been shown to have superior overall numerical performances among the schemes tested.

From the above literature review, it is evident that the upwind schemes are generally more accurate than the simple and efficient centred ones. Recently, a multi-stage (MUSTA) method for the hyperbolic systems of conservation laws has been proposed in the literature [13–15]. The MUSTA method is rather simple for estimating a numerical flux because it does not require the use of the eigenstructure of the governing equations. Hence, the MUSTA method could be widely applicable to the general systems of hyperbolic conservation laws. For the Euler equations, the MUSTA scheme has been shown to combine the simplicity of the centred scheme and the accuracy of the upwind scheme [13].

The purpose of this paper is to propose a finite-volume multi-stage (FMUSTA) scheme for solving 2D SWE with the source terms. The FVM is employed to shorten the 2D problem into a number of local 1D Riemann problems in the direction normal to the cell interface. On the basis of the MUSTA method proposed by Toro and Titarev [15], the numerical flux function of the local Lax–Friedrichs scheme is adopted to establish the first-order monotonic FMUSTA scheme. The second-order-accuracy extension of the proposed FMUSTA scheme is achieved by using the monotonic upstream schemes for conservation laws (MUSCL) method [4]. For the treatment of source terms, the surface gradient method (SGM) proposed by Zhou *et al*. [16] is employed for the data reconstruction of the water level. The proposed first-order and second-order schemes are applied to simulate six shallow-water flows with hydraulic shock waves, including the 1D idealized dam-break flow, the steady transcritical flow over a hump, the 2D oblique hydraulic jump, the circular dam-break flow, the dam-break flow over a hump and the dam-break flow with 90° bend channel.

DOI: 10.1002/fld

2. GOVERNING EQUATIONS

The non-linear system of 2D SWE can be expressed in the conservative form as [17]

$$\frac{\partial \mathbf{Q}}{\partial t}+\frac{\partial \mathbf{F}}{\partial x}+\frac{\partial \mathbf{G}}{\partial y}=\mathbf{S} \tag{1}$$

in which

$$\mathbf{Q}=\begin{bmatrix} h \\ hu \\ hv \end{bmatrix}, \quad \mathbf{F}=\begin{bmatrix} hu \\ hu^2+\dfrac{gh^2}{2} \\ huv \end{bmatrix}, \quad \mathbf{G}=\begin{bmatrix} hv \\ huv \\ hv^2+\dfrac{gh^2}{2} \end{bmatrix}, \quad \mathbf{S}=\begin{bmatrix} 0 \\ gh(s_{0x}-s_{fx}) \\ gh(s_{0y}-s_{fy}) \end{bmatrix} \tag{2}$$

where $\mathbf{Q}$ is the conserved physical vector; $\mathbf{F}$ and $\mathbf{G}$ are the flux vectors in the x- and y-directions, respectively; $\mathbf{S}$ is the source term; h is the water depth; u and v are the depth-averaged velocity components in the x- and y-directions, respectively; g is the gravitational acceleration; s_{0x} and s_{fx} are the bed slope and the friction slope in the x-direction, respectively; and s_{0y} and s_{fy} are the bed slope and the friction slope in the y-direction, respectively. Employing the Manning formula, the friction slopes are

$$s_{fx}=\frac{un_m^2\sqrt{u^2+v^2}}{h^{4/3}}, \quad s_{fy}=\frac{vn_m^2\sqrt{u^2+v^2}}{h^{4/3}} \tag{3}$$

where n_m is the Manning roughness coefficient.

3. FMUSTA SCHEMES

3.1. Cell-centred FVM

The commonly used cell-centred FVM for the discretization of the conservative governing equations is adopted in this paper [5]. Adopting the divergence theorem, the integral form of Equation (1) over an arbitrary control volume Ω is

$$\int\int_{\Omega}\frac{\partial \mathbf{Q}}{\partial t}\,\mathrm{d}W+\int_{\partial\Omega}(\mathbf{F},\mathbf{G})\cdot\mathbf{n}\,\mathrm{d}l=\int\int_{\Omega}\mathbf{S}\,\mathrm{d}W \tag{4}$$

where $\mathrm{d}W$ is the area element; $\partial\Omega$ is the boundary of the control volume Ω; $\mathrm{d}l$ is the arc element; and $\mathbf{n}$ is the outward unit vector normal to the $\partial\Omega$. The vector quantity $\mathbf{Q}$ is assumed to be constant over each cell, leading to the cell-centred FVM. On the basis of the rotational invariance property of the governing equations, Equation (4) is discretized as the basic equation of FVM

$$A\frac{\mathrm{d}\mathbf{Q}}{\mathrm{d}t}+\sum_{m=1}^{M}\mathbf{T}(\theta)^{-1}\mathbf{F}(\overline{\mathbf{Q}})L^m=\widetilde{\mathbf{S}} \tag{5}$$

where A is the area of the cell; m is the index that represents the side of the cell; M is the total number of the sides for the cell; L^m is the length of the m side for the cell; $\widetilde{\mathbf{S}}$ is the integral form of the source terms; $\mathbf{F}(\overline{\mathbf{Q}})=[hu_{\overline{x}}, hu_{\overline{x}}^2+gh^2/2, hu_{\overline{x}}v_{\overline{y}}]^{\mathrm{T}}$ is the normal flux vector for the m side;

DOI: 10.1002/fld

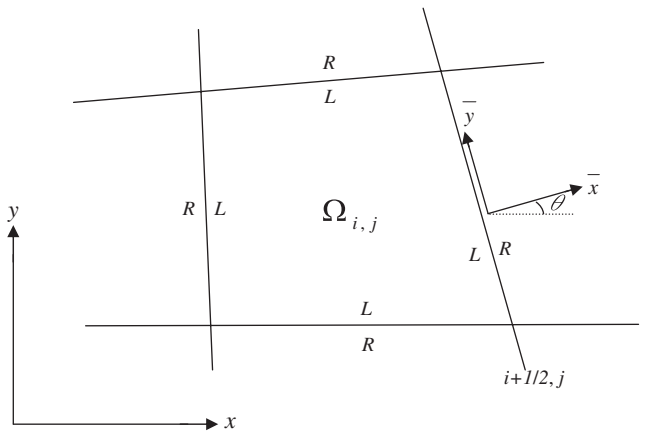

Figure 1. Numerical FVM framework.

$\overline{\mathbf{Q}}=\mathbf{T}(\theta)\mathbf{Q}=[h, hu_{\overline{x}}, hv_{\overline{y}}]^{\mathrm{T}}$ is the vector variables transformed from $\mathbf{Q}$; θ is the angle between the outward unit vector $\mathbf{n}$ and the x-axis; $\mathbf{T}(\theta)$ is the rotation matrix corresponding to the m side; $\mathbf{T}(\theta)^{-1}$ is its inverse [17]; and $u_{\overline{x}}$ and $v_{\overline{y}}$ are, respectively, the velocity components in the $\overline{x}$- and $\overline{y}$-directions, which are denoted as $u_{\overline{x}}=u\cos\theta+v\sin\theta$ and $v_{\overline{y}}=v\cos\theta-u\sin\theta$. On the basis of the FVM, as shown in Figure 1, the numerical flux can be obtained by solving the local 1D Riemann problem in the $\overline{x}$-direction, namely [11]

$$\frac{\partial\overline{\mathbf{Q}}}{\partial t}+\frac{\partial[\mathbf{F}(\overline{\mathbf{Q}})]}{\partial\overline{x}}=0 \tag{6a}$$

with

$$\overline{\mathbf{Q}}(\overline{x},0)=\begin{cases}\overline{\mathbf{Q}}_L, & \overline{x}<0\\ \overline{\mathbf{Q}}_R, & \overline{x}>0\end{cases} \tag{6b}$$

in which $\overline{\mathbf{Q}}_L$ and $\overline{\mathbf{Q}}_R$ represent the initial conserved constant quantities on the left cell L and the right cell R of the cell interface LR, respectively. The resulting first-order finite-volume scheme has the form

$$\mathbf{Q}_{i,j}^{n+1}=\mathbf{Q}_{i,j}^{n}-\left[\frac{\Delta t}{A}\sum_{m=1}^{M}\mathbf{T}(\theta)^{-1}\mathbf{F}^{(1)}L^{m}\right]_{i,j}^{n}+\left(\frac{\Delta t}{A}\widetilde{\mathbf{S}}\right)_{i,j}^{n}=0 \tag{7}$$

where i and j are the space indexes; n is the time index; Δt is the time step; $\mathbf{Q}_{i,j}^{n}$ is the vector of conserved variables for the cell (i, j) at time index n; and $\mathbf{F}^{(1)}$ is the first-order numerical flux.

3.2. MUSTA method

As shown in Equation (7), a monotonic numerical flux $\mathbf{F}^{(1)}$ is required. Toro [13] proposed a rather simple and general MUSTA method for estimating a monotonic numerical flux. This paper directly employs the MUSTA method in FVM framework to estimate a finite-volume numerical flux *via* the predictor and the corrector steps. In the predictor step, the solution of the corresponding

DOI: 10.1002/fld

Riemann problem is numerically approximated to produce two modified states on either side of the cell interface. Then, the corrector step uses a numerical flux function with the two modified states of the predictor step for estimating the numerical flux.

3.2.1. Predictor step. According to the MUSTA method, the solution in Equation (6) is obtained by transforming original Riemann problem in an independent so-called MUSTA mesh, as shown in Figure 2 [15]. The corresponding Riemann problem on the $\overline{d}-\tau$ plane has the form

$$\frac{\partial \overline{\mathbf{Q}}}{\partial \tau}+\frac{\partial[\mathbf{F}(\overline{\mathbf{Q}})]}{\partial \overline{d}}=0 \tag{8a}$$

with

$$\overline{\mathbf{Q}}(\overline{d},0)=\begin{cases}\overline{\mathbf{Q}}_L^n, & \overline{d}<0\\ \overline{\mathbf{Q}}_R^n, & \overline{d}>0\end{cases} \tag{8b}$$

where $\overline{d}$ represents the spatial variable, associated with $\overline{x}$; and τ denotes the temporal variable, associated with t. In the MUSTA mesh as illustrated in Figure 2, the $\overline{d}$-axis is discretized into a number of cells with total number N and regular size $\Delta\overline{d}$. The τ-axis includes a number of time stages with total stage K. Figure 2 also indicates that cells L and R correspond, respectively, to cells 0 and 1 in the MUSTA mesh. Thus, the numerical flux at interface LR in Equation (7) corresponds to the one at interface $\frac{1}{2}$ in the MUSTA mesh.

For approximating the solution of the Riemann problem (8), the initial condition in the MUSTA mesh is defined as

$$\overline{\mathbf{Q}}_l^{(0)}=\begin{cases}\overline{\mathbf{Q}}_L^n, & l\leqslant 0\\ \overline{\mathbf{Q}}_R^n, & l\geqslant 1\end{cases} \tag{9}$$

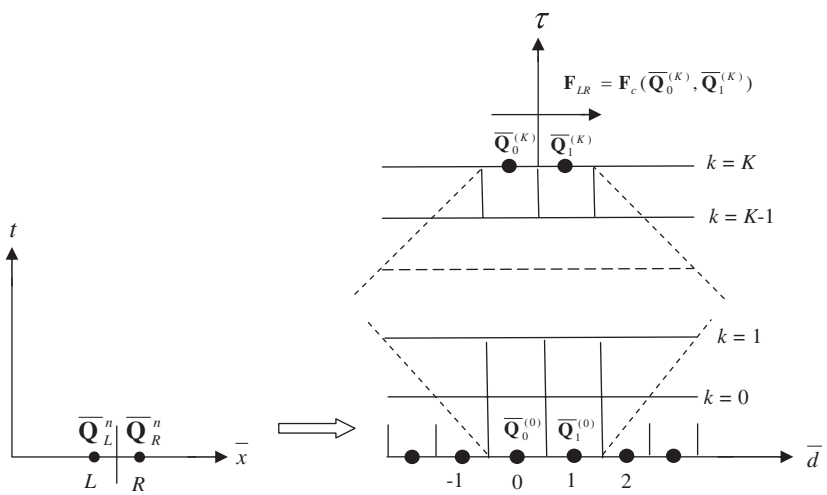

Figure 2. The MUSTA method in the FVM framework.

DOI: 10.1002/fld

in which l represents the space index in the MUSTA mesh. The τ-time evolution of the problem is advanced to obtain the local solution by the use of the conservative formula

$$\overline{\mathbf{Q}}_l^{(k+1)} = \overline{\mathbf{Q}}_l^{(k)} - \left(\frac{\Delta\tau}{\Delta\overline{d}}\right)^{(k)} [(\mathbf{F}_\mathrm{p})_{l+1/2}^{(k)} - (\mathbf{F}_\mathrm{p})_{l-1/2}^{(k)}] \tag{10}$$

where $\Delta\tau$ is the time step in the MUSTA mesh and $\mathbf{F}_\mathrm{p}$ is a two-point monotonic numerical flux, namely the MUSTA predictor flux. After a prescribed number of stages K with time evolution of the solution, the predictor step is performed and two new interface states $\overline{\mathbf{Q}}_0^{(K)}$ and $\overline{\mathbf{Q}}_1^{(K)}$ are obtained on the MUSTA mesh.

3.2.2. Corrector step. With $\overline{\mathbf{Q}}_0^{(K)}$ and $\overline{\mathbf{Q}}_1^{(K)}$, the numerical flux $\mathbf{F}_{LR}^{(K)}$ for interface LR is estimated by using a specified two-point monotonic numerical flux $\mathbf{F}_\mathrm{c}$, namely the MUSTA corrector flux:

$$\mathbf{F}_{LR}^{(K)} = \mathbf{F}_\mathrm{c}(\overline{\mathbf{Q}}_0^{(K)}, \overline{\mathbf{Q}}_1^{(K)}) \tag{11}$$

Finally, using the numerical flux $\mathbf{F}^{(1)} = \mathbf{F}_{LR}^{(K)}$, Equation (7) leads to a first-order monotonic numerical scheme, namely the FMUSTA scheme.

As described in Sections 3.2.1, the MUSTA method requires the choice of the number of stages K. In theory, the larger the number of stages, the closer the resulting numerical flux is to the Godunov flux of the exact Riemann solver. Nevertheless, according to Toro and Titarev [15] the choice $K = 1$ is recommended for practical applications.

3.2.3. FMUSTA scheme (K = 1). As illustrated in Figure 2, the MUSTA method requires a number of cells N, stages K and the numerical boundary conditions. The simplest choice is the one-stage ($K = 1$) approach, in which the two cells (0 and 1) are adopted. The boundary fluxes are estimated on the nearest cells in the interior of the computational domain. This treatment is efficient and does not result in much loss of the numerical accuracy [15]. As shown in Figure 3, as $K = 1$ the initial data in the one-stage MUSTA method are prescribed in the domain of just two cells, namely $l = 0$ and $l = 1$. Therefore, the simplest one-stage MUSTA method is advanced using the conservative Equation (10) to construct the two new interface states $\overline{\mathbf{Q}}_0^{(1)}$ and $\overline{\mathbf{Q}}_1^{(1)}$:

$$\overline{\mathbf{Q}}_0^{(1)} = \overline{\mathbf{Q}}_0^{(0)} - \left(\frac{\Delta\tau}{\Delta\overline{d}}\right)^{(0)} [(\mathbf{F}_\mathrm{p})_{1/2}^{(0)} - (\mathbf{F}_\mathrm{p})_{-1/2}^{(0)}] \tag{12a}$$

$$\overline{\mathbf{Q}}_1^{(1)} = \overline{\mathbf{Q}}_1^{(0)} - \left(\frac{\Delta\tau}{\Delta\overline{d}}\right)^{(0)} [(\mathbf{F}_\mathrm{p})_{3/2}^{(0)} - (\mathbf{F}_\mathrm{p})_{1/2}^{(0)}] \tag{12b}$$

where the MUSTA predictor flux at interface $\frac{1}{2}$ has the form:

$$(\mathbf{F}_\mathrm{p})_{1/2}^{(0)} = \mathbf{F}_\mathrm{p}(\overline{\mathbf{Q}}_0^{(0)}, \overline{\mathbf{Q}}_1^{(0)}) = \mathbf{F}_\mathrm{p}(\overline{\mathbf{Q}}_L^n, \overline{\mathbf{Q}}_R^n) \tag{13}$$

DOI: 10.1002/fld

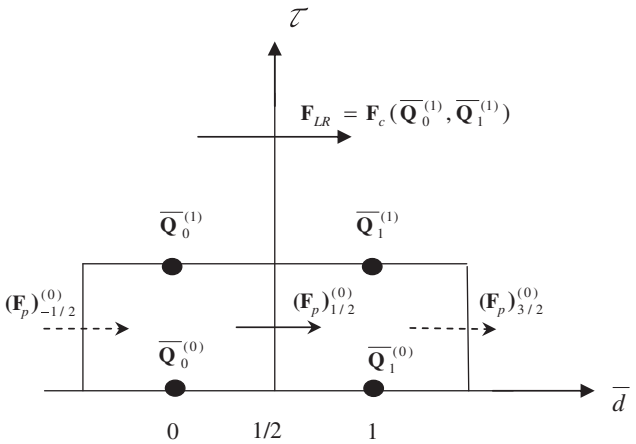

Figure 3. Example of a MUSTA method ($K=1$).

The boundary fluxes $(\mathbf{F}_\mathrm{p})_{-1/2}^{(0)}$ and $(\mathbf{F}_\mathrm{p})_{3/2}^{(0)}$, denoted by the dashed-line arrows in Figure 3, are computed with the initial data expressed in Equation (9)

$$(\mathbf{F}_\mathrm{p})_{-1/2}^{(0)} = \mathbf{F}(\overline{\mathbf{Q}}_0^{(0)}) = \mathbf{F}(\overline{\mathbf{Q}}_L^n) \tag{14a}$$

$$(\mathbf{F}_\mathrm{p})_{3/2}^{(0)} = \mathbf{F}(\overline{\mathbf{Q}}_1^{(0)}) = \mathbf{F}(\overline{\mathbf{Q}}_R^n) \tag{14b}$$

By following Toro and Titarev [15], the time step $\Delta\tau^{(0)}$ in one-stage MUSTA method has the form

$$\Delta\tau^{(0)} = \frac{\mathrm{CFL}\Delta\overline{d}^{(0)}}{c_{\max}^{(0)}} \tag{15}$$

in which CFL represents the Courant–Friedrichs–Lewy stability coefficient; and $c_{\max}^{(0)}$ is the maximum signal speed in the MUSTA mesh at initial stage. For the 2D SWE, $c_{\max}^{(0)}$ denotes the maximum wave-propagation speed and can be expressed as

$$c_{\max}^{(0)} = \max(|u_{\overline{x}} + \sqrt{gh}|_1^{(0)},\ |u_{\overline{x}} + \sqrt{gh}|_0^{(0)}) \tag{16}$$

Substituting Equations (9) and (13)–(15) into Equation (12) one obtains

$$\overline{\mathbf{Q}}_0^{(1)} = \overline{\mathbf{Q}}_L^n - \frac{\mathrm{CFL}}{c_{\max}^{(0)}}[\mathbf{F}_\mathrm{p}(\overline{\mathbf{Q}}_L^n, \overline{\mathbf{Q}}_R^n) - \mathbf{F}(\overline{\mathbf{Q}}_L^n)] \tag{17a}$$

$$\overline{\mathbf{Q}}_1^{(1)} = \overline{\mathbf{Q}}_R^n - \frac{\mathrm{CFL}}{c_{\max}^{(0)}}[\mathbf{F}(\overline{\mathbf{Q}}_R^n) - \mathbf{F}_\mathrm{p}(\overline{\mathbf{Q}}_L^n, \overline{\mathbf{Q}}_R^n)] \tag{17b}$$

As $K=1$ expressed in Equation (17), the MUSTA method is completely performed. With the two new interface states $\overline{\mathbf{Q}}_0^{(1)}$ and $\overline{\mathbf{Q}}_1^{(1)}$, the monotonic numerical flux is achieved by employing the MUSTA corrector flux:

$$\mathbf{F}_{LR}^{(1)} = \mathbf{F}_\mathrm{c}(\overline{\mathbf{Q}}_0^{(1)}, \overline{\mathbf{Q}}_1^{(1)}) \tag{18}$$

Finally, with the numerical flux $\mathbf{F}^{(1)} = \mathbf{F}_{LR}^{(1)}$ one obtains the one-stage FMUSTA scheme ($K=1$).

DOI: 10.1002/fld

3.2.4. Predictor and corrector fluxes. To completely estimate the numerical flux, the MUSTA predictor and corrector fluxes are required. In order to achieve simplicity and generality, the most general choice is to utilize a simple and efficient flux both for the predictor and the corrector fluxes [15]. Thus, the local Lax–Friedrichs flux estimation, which has been proven to be the simplest and the most efficient among several commonly used schemes by Lai *et al.* [11], is employed herein. Using the local Lax–Friedrichs numerical flux function [11, 18], the MUSTA predictor and corrector fluxes are, respectively,

$$\mathbf{F}_{\mathrm{p}}(\overline{\mathbf{Q}}_L^n, \overline{\mathbf{Q}}_R^n) = \frac{1}{2}[\mathbf{F}(\overline{\mathbf{Q}}_L^n) + \mathbf{F}(\overline{\mathbf{Q}}_R^n)] - \frac{1}{2}\frac{c_{\max}^{(0)}}{\mathrm{CFL}}(\overline{\mathbf{Q}}_R^n - \overline{\mathbf{Q}}_L^n) \tag{19a}$$

$$\mathbf{F}_{\mathrm{c}}(\overline{\mathbf{Q}}_0^{(1)}, \overline{\mathbf{Q}}_1^{(1)}) = \frac{1}{2}[\mathbf{F}(\overline{\mathbf{Q}}_0^{(1)}) + \mathbf{F}(\overline{\mathbf{Q}}_1^{(1)})] - \frac{1}{2}\frac{c_{\max}^{(1)}}{\mathrm{CFL}}(\overline{\mathbf{Q}}_1^{(1)} - \overline{\mathbf{Q}}_0^{(1)}) \tag{19b}$$

$$c_{\max}^{(1)} = \max(|u_{\overline{x}} + \sqrt{gh}|_1^{(1)}, |u_{\overline{x}} + \sqrt{gh}|_0^{(1)}) \tag{19c}$$

Finally, the algorithm for estimating the numerical flux in the one-stage FMUSTA scheme ($K=1$) is summarized as follows:

1. Using Equation (19a), one obtains the predictor flux at local interface $\frac{1}{2}$.
2. Employing Equation (17), one obtains two new interface states $\overline{\mathbf{Q}}_0^{(1)}$ and $\overline{\mathbf{Q}}_1^{(1)}$.
3. With $\overline{\mathbf{Q}}_0^{(1)}$ and $\overline{\mathbf{Q}}_1^{(1)}$, Equation (19b) leads to the one-stage numerical flux $\mathbf{F}_{LR}^{(1)} = \mathbf{F}_{\mathrm{c}}(\overline{\mathbf{Q}}_0^{(1)}, \overline{\mathbf{Q}}_1^{(1)})$.
4. As $\mathbf{F}^{(1)} = \mathbf{F}_{LR}^{(1)}$, Equation (7) leads to the one-stage FMUSTA scheme ($K=1$).

Note that as $K=0$, Equation (7) leads to the original local Lax–Friedrichs scheme.

The procedure to estimate the numerical flux in the k-stage FMUSTA scheme with two cells (0 and 1) is also described herein. The MUSTA is started by setting $\overline{\mathbf{Q}}_0^{(0)} = \overline{\mathbf{Q}}_L^n$ and $\overline{\mathbf{Q}}_1^{(0)} = \overline{\mathbf{Q}}_R^n$ for initial stage $k=0$. Then, for $0 \leqslant k \leqslant K-1$, where K is the desired number of stages, the algorithm is summarized as follows:

1. Employ the local Lax–Friedrichs numerical flux function to estimate the numerical flux at the stage k as:

$$\mathbf{F}_{1/2}^{(k)} = \frac{1}{2}[\mathbf{F}(\overline{\mathbf{Q}}_0^{(k)}) + \mathbf{F}(\overline{\mathbf{Q}}_1^{(k)})] - \frac{1}{2}\frac{c_{\max}^{(k)}}{\mathrm{CFL}}(\overline{\mathbf{Q}}_1^{(k)} - \overline{\mathbf{Q}}_0^{(k)}) \tag{20a}$$

$$c_{\max}^{(k)} = \max(|u_{\overline{x}} + \sqrt{gh}|_1^{(k)}, |u_{\overline{x}} + \sqrt{gh}|_0^{(k)}) \tag{20b}$$

2. Update the left and right data by

$$\overline{\mathbf{Q}}_0^{(k+1)} = \overline{\mathbf{Q}}_0^{(k)} - \frac{\mathrm{CFL}}{c_{\max}^{(k)}}[\mathbf{F}_{1/2}^{(k)} - \mathbf{F}(\overline{\mathbf{Q}}_0^{(k)})] \tag{21a}$$

$$\overline{\mathbf{Q}}_1^{(k+1)} = \overline{\mathbf{Q}}_1^{(k)} - \frac{\mathrm{CFL}}{c_{\max}^{(k)}}[\mathbf{F}(\overline{\mathbf{Q}}_1^{(k)}) - \mathbf{F}_{1/2}^{(k)}] \tag{21b}$$

3. Goto step 1.

DOI: 10.1002/fld

The procedure is stopped at the end of step 1 if the desired number of stages has been reached. The final flux in the k-stage FMUSTA scheme is given by $\mathbf{F}^{(1)}=\mathbf{F}_{LR}^{(K)}=\mathbf{F}_{1/2}^{(K)}$.

3.3. Second-order extension

The MUSCL method [4] is adopted herein for establishing the second-order extension of the proposed FMUSTA scheme. The extension consists of two steps, a predictor and a corrector. In the predictor step, the first-order numerical flux $\mathbf{F}^{(1)}$ is used to advance the intermediate values over a half time step. In the corrector step, the second-order numerical flux $\mathbf{F}^{(2)}$ is adopted to achieve the final solution over a time step. The resulting scheme has the following form:

$$\mathbf{Q}_{i,j}^{n+1/2}=\mathbf{Q}_{i,j}^{n}-\left[\frac{\Delta t}{2A}\sum_{m=1}^{M}\mathbf{T}(\theta)^{-1}\mathbf{F}^{(1)}L^{m}\right]_{i,j}^{n}+\left(\frac{\Delta t}{2A}\widetilde{\mathbf{S}}\right)_{i,j}^{n} \tag{22a}$$

$$\mathbf{Q}_{i,j}^{n+1}=\mathbf{Q}_{i,j}^{n}-\left[\frac{\Delta t}{A}\sum_{m=1}^{M}\mathbf{T}(\theta)^{-1}\mathbf{F}^{(2)}L^{m}\right]_{i,j}^{n+1/2}+\left(\frac{\Delta t}{A}\widetilde{\mathbf{S}}\right)_{i,j}^{n+1/2} \tag{22b}$$

In Equation (22), the first-order numerical flux $\mathbf{F}^{(1)}$ is obtained by the MUSTA method with two initial constant values $\overline{\mathbf{Q}}_L^n$ and $\overline{\mathbf{Q}}_R^n$. For the second-order numerical flux $\mathbf{F}^{(2)}$, the constant values are reconstructed using the MUSCL method. By introducing a non-linear slope limiter function to avoid the numerical oscillations, the reconstructed values of conserved variables on the left and right of the cell interface $(i+1/2, j)$, respectively, have the form

$$\mathbf{Q}_{i+1/2,j}^{L}=\mathbf{T}(\theta)(\mathbf{Q}_{i,j}^{n+1/2}+\tfrac{1}{2}\Delta_{i,j}^{n+1/2}) \tag{23a}$$

$$\mathbf{Q}_{i+1/2,j}^{R}=\mathbf{T}(\theta)(\mathbf{Q}_{i+1,j}^{n+1/2}-\tfrac{1}{2}\Delta_{i+1,j}^{n+1/2}) \tag{23b}$$

in which $\Delta_{i,j}=\Delta_{i,j}(\Delta_{i+1/2,j},\Delta_{i-1/2,j})$ represents the non-linear slope limiter function and several different forms of slope limiters can be employed [4]. The Roe symmetric limiter function [19] is adopted herein

$$\Delta_{i,j}=\begin{cases}\Delta_{i+1/2,j} & \text{if } |\Delta_{i+1/2,j}|<|\Delta_{i-1/2,j}|\\ \Delta_{i-1/2,j} & \text{otherwise}\end{cases} \tag{24}$$

where $\Delta_{i+1/2,j}=\mathbf{Q}_{i+1,j}^{n+1/2}-\mathbf{Q}_{i,j}^{n+1/2}$ and $\Delta_{i-1/2,j}=\mathbf{Q}_{i,j}^{n+1/2}-\mathbf{Q}_{i-1,j}^{n+1/2}$. With the left and right reconstructed cell-interface variables expressed in Equation (23), the second-order numerical flux through the cell interface $(i+1/2, j)$ can be directly obtained by employing the MUSTA method described in Sections 3.1–3.2. On the basis of the MUSCL method, the resulting second-order extension of the proposed FMUSTA scheme is referred to as the FMUSTA-MUSCL scheme in this paper.

3.4. Treatment of source terms

Modeling shallow-water flows with the presence of the bed slope and friction slope numerically requires the proper treatment of source terms in 2D SWE [20]. Recently, different methods have been proposed to cope with the source terms [20–25]. The SGM proposed by Zhou *et al.* [16] has been shown to be simple, and it can be well implemented in the MUSCL method. In the

DOI: 10.1002/fld

present study, the SGM is adopted in the data reconstruction of Equation (23). On the basis of the SGM, the left and right water levels, $\eta^L_{i+1/2,j}$ and $\eta^R_{i+1/2,j}$, of the cell interface $(i+1/2, j)$ are reconstructed using Equation (23). Then, the left and right cell interface $(i+1/2, j)$ water depths, $h^L_{i+1/2,j}$ and $h^R_{i+1/2,j}$, are, respectively,

$$h^L_{i+1/2,j}=\eta^L_{i+1/2,j}-z_{bi+1/2,j}, \quad h^R_{i+1/2,j}=\eta^R_{i+1/2,j}-z_{bi+1/2,j} \tag{25}$$

where $z_{bi+1/2,j}$ is the bed elevation at the cell interface $(i+1/2, j)$. The velocities are then reconstructed as

$$(u_{\overline{x}})^L_{i+1/2,j}=(hu_{\overline{x}})^L_{i+1/2,j}/h^L_{i+1/2,j}, \quad (u_{\overline{x}})^R_{i+1/2,j}=(hu_{\overline{x}})^R_{i+1/2,j}/h^R_{i+1/2,j} \tag{26a}$$

$$(v_{\overline{y}})^L_{i+1/2,j}=(hv_{\overline{y}})^L_{i+1/2,j}/h^L_{i+1/2,j}, \quad (v_{\overline{y}})^R_{i+1/2,j}=(hv_{\overline{y}})^R_{i+1/2,j}/h^R_{i+1/2,j} \tag{26b}$$

For the discretization of the bed slope source terms, the divergence theorem is used to calculate [26]

$$\frac{\partial z_b}{\partial x}=\frac{(z_{b1}-z_{b3})(y_2-y_4)-(z_{b2}-z_{b4})(y_1-y_3)}{(x_1-x_3)(y_2-y_4)-(x_2-x_4)(y_1-y_3)} \tag{27a}$$

$$\frac{\partial z_b}{\partial y}=\frac{(z_{b1}-z_{b3})(x_2-x_4)-(z_{b2}-z_{b4})(x_1-x_3)}{(y_1-y_3)(x_2-x_4)-(y_2-y_4)(x_1-x_3)} \tag{27b}$$

where the subscripts $1, 2, 3$, and 4, respectively, represent the node numbers of the cell (i, j). Therefore, the x and y components of the source terms $\widetilde{\mathbf{S}}$ in Equation (22) are, respectively, discretized as:

$$\widetilde{S}_x=-gh_{i,j}A_{i,j}\left[\frac{(z_{b1}-z_{b3})(y_2-y_4)-(z_{b2}-z_{b4})(y_1-y_3)}{(x_1-x_3)(y_2-y_4)-(x_2-x_4)(y_1-y_3)}+\frac{u_{i,j}n^2_{m_{i,j}}\sqrt{u^2_{i,j}+v^2_{i,j}}}{h^{4/3}_{i,j}}\right] \tag{28a}$$

$$\widetilde{S}_y=-gh_{i,j}A_{i,j}\left[\frac{(z_{b1}-z_{b3})(x_2-x_4)-(z_{b2}-z_{b4})(x_1-x_3)}{(y_1-y_3)(x_2-x_4)-(y_2-y_4)(x_1-x_3)}+\frac{v_{i,j}n^2_{m_{i,j}}\sqrt{u^2_{i,j}+v^2_{i,j}}}{h^{4/3}_{i,j}}\right] \tag{28b}$$

3.5. Stability and boundary conditions

For the numerical stability requirement, the time step Δt must be restricted by the CFL condition [27]. The time step is limited by

$$\Delta t\leqslant \mathrm{CFL}\min\left(\frac{d_{i,j}}{\max(\sqrt{u^2+v^2}+\sqrt{gh})_{i,j}}\right) \tag{29}$$

where $d_{i,j}$ denotes the whole set of distances between the i, jth centroid and the centroids of the four adjacent cells. As $\mathrm{CFL}=1$, Equation (29) gives rise to a maximum allowable time step.

The boundary conditions used herein include the land boundary and the open boundary. At the land boundary, the velocity normal to the land is set to be zero such that no flux occurs through the boundary. The open boundary conditions are set by the use of the outgoing Riemann invariants. For a detailed description about the adopted boundary conditions used herein one can be refer to Reference [18].

DOI: 10.1002/fld

4. NUMERICAL RESULTS AND DISCUSSIONS

The numerical performances of the first-order and second-order proposed schemes with different numbers of stages K are evaluated using the six shallow-water flow simulations, namely the 1D idealized dam-break flow, the steady transcritical flow over a hump, the 2D oblique hydraulic jump, the circular dam-break flow, the dam-break flow over a hump and the dam-break flow with a 90° bend channel. Two commonly used upwind schemes, namely the Roe scheme and the HLL scheme, are adopted herein to compare with the proposed FMUSTA schemes. All of the tests were performed on a Pentium IV equipped with a 1 gigabyte RAM.

4.1. 1D idealized dam-break flow

The purpose of the 1D idealized dam-break test problem is to assess the performances of the proposed FMUSTA schemes in resolving the shock waves, in which it is well known that the non-monotonic scheme presents spurious oscillations around shocks. The present test is the dam-break flow over a rectangular, frictionless and horizontal channel with 2000 m length and 10 m width. The initial conditions consist of two constant still water depths separated by a dam located at the middle of the channel. The initial upstream water depth h_{us} is 10 m, and downstream water depths h_{ds} are 5 and 0.1 m, respectively. Hence, two initial water-depth ratios h_{ds}/h_{us} of 0.5 and 0.01 are tested. Hundred computational cells (i.e. grid spacing Δx of 20 m) are used. The CFL number is set to be 0.9 for all the tests. The simulation time is 50 s after the dam breaks.

4.1.1. Effect of stage number K. As described in Section 3.2, the usage of the different stage number K in the MUSTA method can result in different numerical performances of the proposed FMUSTA scheme. To show the influence of stage number on the simulated results, three different numbers of stages, $K=1, 2$ and 3, are considered herein. Figure 4 shows the influence of K on the simulated water depth for the test case with a water-depth ratio of 0.01. It is clear that the proposed FMUSTA schemes can capture the shock and the rarefaction wave without any spurious oscillation. The result also indicates that the proposed two-stage ($K=2$) and three-stage ($K=3$) FMUSTA schemes present almost the same resolutions, and they seem more accurate than the one-stage FMUSTA scheme ($K=1$).

To evaluate the numerical accuracy quantitatively, three different error norms, L_1, L_2 and L_∞, are used herein [6]

$$L_1=\frac{\sum|Y_{i,j}^{\text{sim}}-Y_{i,j}^{\text{exact}}|}{\sum|Y_{i,j}^{\text{exact}}|},\quad L_2=\sqrt{\frac{\sum(Y_{i,j}^{\text{sim}}-Y_{i,j}^{\text{exact}})^2}{\sum(Y_{i,j}^{\text{exact}})^2}},\quad L_\infty=\frac{\max|Y_{i,j}^{\text{sim}}-Y_{i,j}^{\text{exact}}|}{\max|Y_{i,j}^{\text{exact}}|} \tag{30}$$

where $Y_{i,j}^{\text{sim}}$ and $Y_{i,j}^{\text{exact}}$ are the simulated solution and the exact solution at cell (i, j), respectively. Table I summarizes the error norms of the water depth and CPU time for water-depth ratios of 0.01. As listed in Table I, the proposed three-stage FMUSTA scheme yields the smallest error norms of L_1, L_2 and L_∞; however, it also consumes the largest CPU time. The two-stage and three-stage FMUSTA schemes are, respectively, about 13 and 26% more expensive than the one-stage FMUSTA scheme. According to CPU-time consumption, the one-stage FMUSTA scheme ($K=1$) is more efficient for practical applications, and it is adopted for the following numerical simulations.

DOI: 10.1002/fld

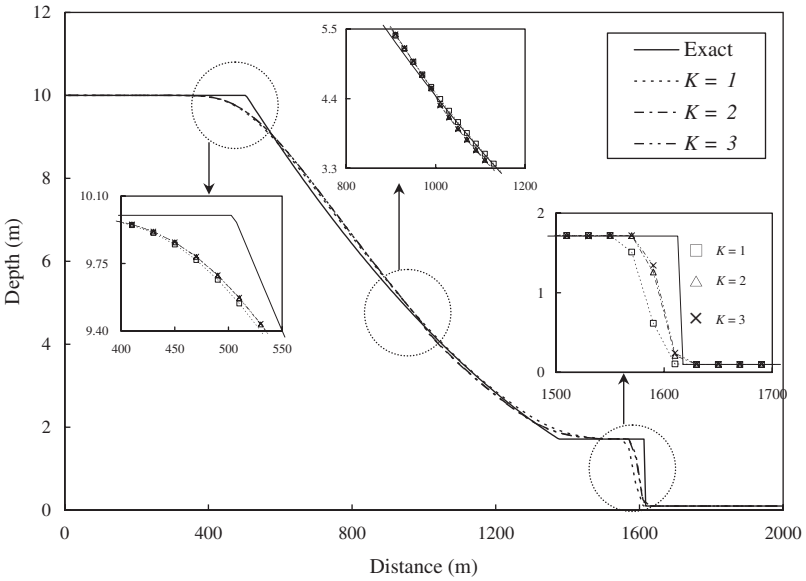

Figure 4. The influence of stage number K on the simulated water depths for a water-depth ratio of 0.01.

Table I. The L_1, L_2, L_∞ norms and the CPU-time consumptions by the proposed FMUSTA schemes with different numbers of stages K for the idealized dam-break problem.

Scheme	L_1	L_2	L_∞	CPU (s)
FMUSTA ($K=1$)	0.0174	0.0345	0.161	0.039
FMUSTA ($K=2$)	0.0166	0.0297	0.149	0.044
FMUSTA ($K=3$)	0.0165	0.0292	0.146	0.049

4.1.2. Comparison of first-order schemes. Employing the one-stage FMUSTA scheme, the simulated results for the water-depth ratios of 0.5 are displayed in Figure 5. The exact solution [28] and the simulated results by the commonly used Roe and HLL schemes are also plotted for comparison. As illustrated in Figure 5 with the close-up of the head of the rarefaction wave, the FMUSTA scheme produces the best resolution. With the close-up of the shock front, the FMUSTA and Roe schemes obtain similar shock-capturing resolutions and they are more accurate than the HLL scheme.

For the water-depth ratio of 0.01, the purpose of this test case is to evaluate the performance of the proposed scheme in simulating the transcritical flows, in which the exact flow condition at the dam site is critical (i.e. Froude number of 1.0) [28]. It is well known that the Roe scheme requires the entropy fix to avoid the apparently entropy-violating solution. Thus, the Roe scheme with the entropy correction [4] is adopted herein for comparison. Figure 6 shows the comparison of the exact solutions with the simulated water depths using the one-stage FMUSTA, Roe with entropy fix and HLL schemes for the water-depth ratio of 0.01. From the simulated results, it is found that the FMUSTA and HLL schemes present similar resolutions near the shock fronts. In addition, the

DOI: 10.1002/fld

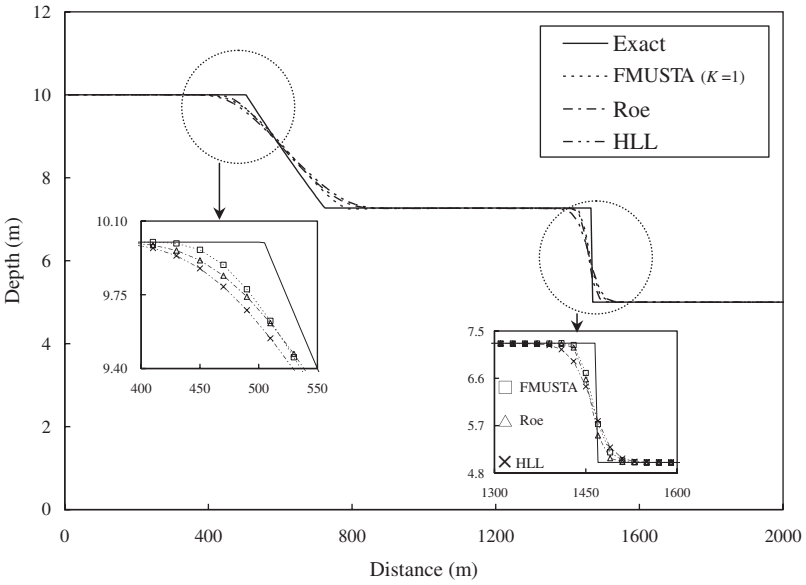

Figure 5. Comparisons of exact solutions with simulated depths using first-order schemes for a water-depth ratio of 0.5.

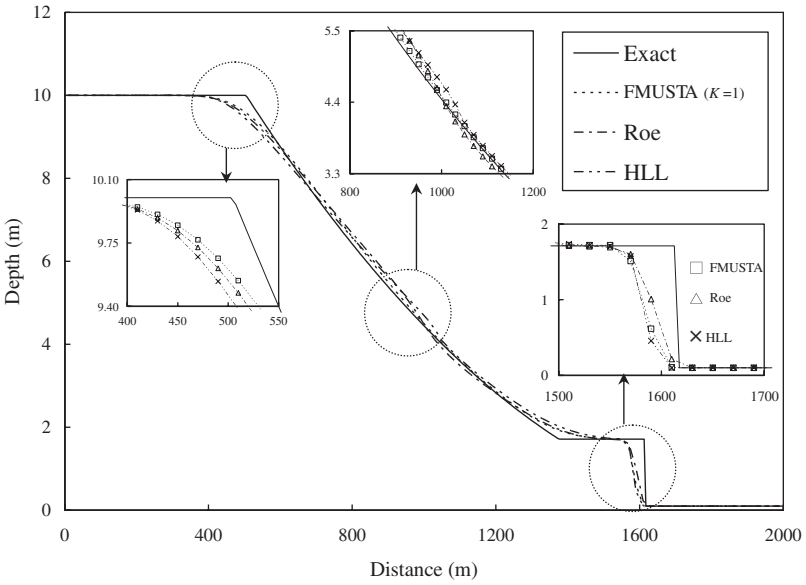

Figure 6. Comparisons of exact solutions with simulated depths using first-order schemes for a water-depth ratio of 0.01.

DOI: 10.1002/fld

Table II. The L_1, L_2, L_∞ norms and the CPU-time consumptions by the first-order upwind schemes for the idealized dam-break problem.

Scheme	L_1	L_2	L_∞	CPU (s)
FMUSTA ($K=1$)	0.0174	0.0345	0.161	0.039
Roe	0.0211	0.0340	0.149	0.047
HLL	0.0254	0.0405	0.161	0.032

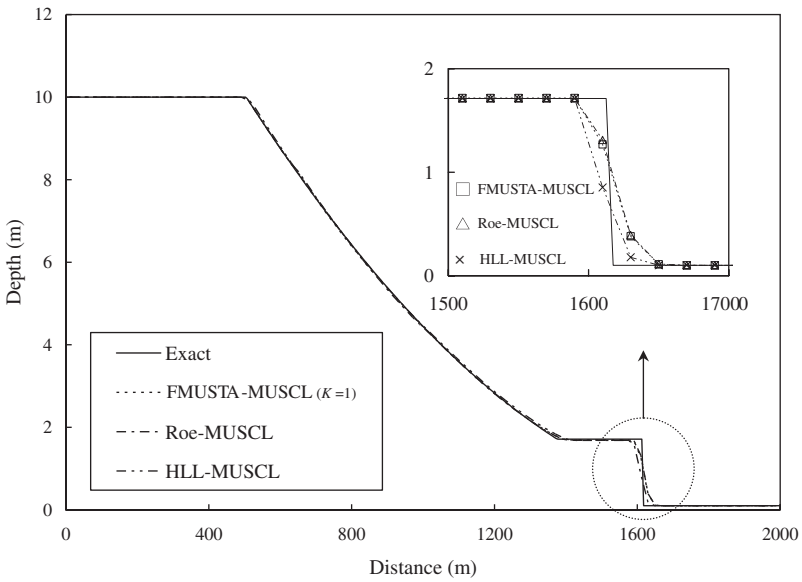

Figure 7. Comparisons of exact solutions with simulated water depths using second-order schemes for a water-depth ratio of 0.01.

FMUSTA scheme obtains the best resolution at the head of the rarefaction wave. At the critical point (i.e. the dam site) the solution by the FMUSTA scheme is very smooth and more accurate than those by the Roe and the HLL schemes. The results indicate that the FMUSTA scheme does not require the special treatment of entropy fixes and yet obtain good solutions automatically for the class of dam-break problems with critical points at the dam site.

From the quantitative results listed in Table II, the Roe scheme was found to have the smallest error norms of L_∞. It implies that the Roe scheme achieves best accurate shock-capturing resolutions among the one-stage FMUSTA, Roe and HLL schemes. However, the CPU time consumed by the Roe scheme is the largest among the schemes tested. Table II also shows that the proposed FMUSTA scheme achieves satisfactory overall numerical accuracy and efficiency compared with the Roe and HLL schemes.

4.1.3. Comparison of second-order schemes. The proposed second-order FMUSTA-MUSCL scheme ($K=1$) is tested and compared with the commonly adopted second-order schemes, namely

DOI: 10.1002/fld

Table III. The L_1, L_2, L_∞ norms and the CPU-time consumptions by the second-order schemes for the idealized dam-break problem.

Scheme	L_1	L_2	L_∞	CPU (s)
FMUSTA-MUSCL ($K=1$)	0.0032	0.0086	0.044	0.083
Roe-MUSCL	0.0035	0.0083	0.041	0.099
HLL-MUSCL	0.0052	0.0143	0.086	0.069

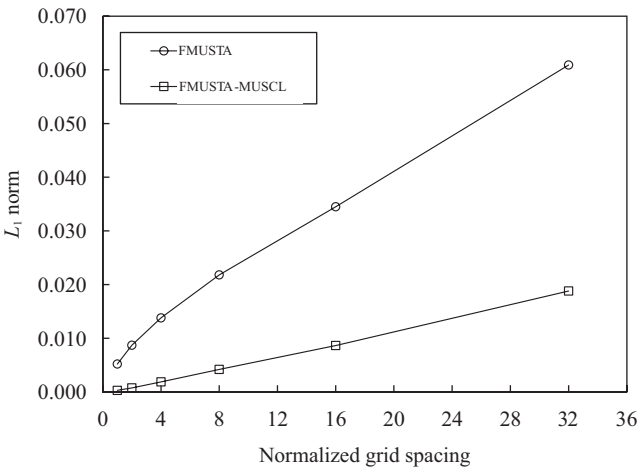

Figure 8. Convergence curves using the proposed FMUSTA and FMUSTA-MUSCL schemes ($K=1$) for a water-depth ratio of 0.01.

the Roe-MUSCL and HLL-MUSCL schemes, for the water-depth ratio of 0.01. All second-order schemes tested herein are based on the MUSCL method with the slope limiter function presented in Equation (24). Comparison of the exact solutions with the simulated water depths using the three second-order upwind schemes is shown in Figure 7. On the basis of the quantitative results for error norms and CPU time consumed in Table III, the proposed FMUSTA-MUSCL scheme was found to achieve satisfactory overall numerical accuracy and efficiency compared with the Roe-MUSCL and the HLL-MUSCL schemes.

4.1.4. Grid refinement effect. A grid convergence study is performed herein to further investigate the influence of the grid spacing on the numerical performance. The proposed one-stage FMUSTA and FMUSTA-MUSCL schemes are adopted for the test case of the water-depth ratio of 0.01. Table IV lists the grid information, the L_1 norms and the order of accuracy p [6]

$$p=\frac{\log(L_{1\text{fine}})-\log(L_{1\text{coarse}})}{\log(\Delta x_{\text{fine}})-\log(\Delta x_{\text{coarse}})} \tag{31}$$

in which $L_{1\text{fine}}$ and $L_{1\text{coarse}}$ represent the L_1 norms computed by the fine and coarse grids, respectively; Δx_{fine} and Δx_{coarse} denote the grid spacing of the fine and coarse grids, respectively. Figure 8 shows the convergence curves for the FMUSTA and FMUSTA-MUSCL schemes with

DOI: 10.1002/fld

Table IV. The L_1 norms and the order of accuracy p for the idealized dam-break problem using the proposed FMUSTA and FMUSTA-MUSCL schemes ($K=1$).

		FMUSTA ($K=1$)		FMUSTA-MUSCL ($K=1$)	
Number of cells	Grid spacing	L_1	p	L_1	p
50	40	0.0609	—	0.01879	—
100	20	0.0345	0.82	0.00864	1.12
200	10	0.0218	0.66	0.00419	1.04
400	5	0.0138	0.66	0.00187	1.16
800	2.5	0.0087	0.67	0.00075	1.32
1600	1.25	0.0052	0.74	0.00029	1.37

the different grid spacings, which is normalized by the finest grid spacing (i.e. $\Delta x = 1.25\,\text{m}$). The results demonstrate that both proposed schemes converge correctly to the exact solution as the grid spacing becomes smaller. With the smallest grid spacing tested, an almost grid-independent solution is obtained by the FMUSTA-MUSCL scheme. For all of the tested grid spacing, as shown in Table IV, the order of accuracy computed from the FMUSTA scheme is on an average about 0.71 and lower than the theoretical order of accuracy (i.e. $p=1$). For the FMUSTA-MUSCL scheme, the average order of accuracy is about 1.2, which is also lower than the theoretical one (i.e. $p=2$). The discrepancy between the computed and the theoretical values may be due to the non-linearity of the solution, the presence of discontinuity and perhaps other factors [6].

4.2. Steady transcritical flow over a hump

The purpose of the steady transcritical flow simulation is to assess the performances of the proposed FMUSTA schemes for capturing the hydraulic shocks with an uneven bed. The test problem has the hump on the bed with elevation variations as a function of [16]

$$z_b(x) = \begin{cases} 0 & \text{if } x < 8\,\text{m} \\ 0.2 - 0.05(x-10)^2 & \text{if } 8 \leqslant x \leqslant 12\,\text{m} \\ 0 & \text{if } x > 12\ \text{m} \end{cases} \tag{32}$$

The frictionless and rectangular channel with 25 m length and 1 m width is considered. Two hundred computational cells are used and the computational time step is set to be 0.02 s. A discharge per unit width of $0.18\,\text{m}^2/\text{s}$ is specified at the upstream boundary and a water depth of 0.33 m is imposed at the downstream boundary.

Employing the one-stage FMUSTA and FMUSTA-MUSCL schemes, the simulated water levels, Froude numbers and discharges per unit width compared with the exact solutions are shown in Figures 9(a), (b) and (c), respectively. According to the exact solution [29], the critical flow is produced at the top of the hump due to the given boundary conditions, as illustrated in Figure 9(b). The simulated transition with a shock (hydraulic jump) by the proposed schemes is well predicted without the spurious oscillations. The proposed FMUSTA-MUSCL produces more accurate solutions than those by the FMUSTA scheme, especially for resolutions of the Froude number

DOI: 10.1002/fld

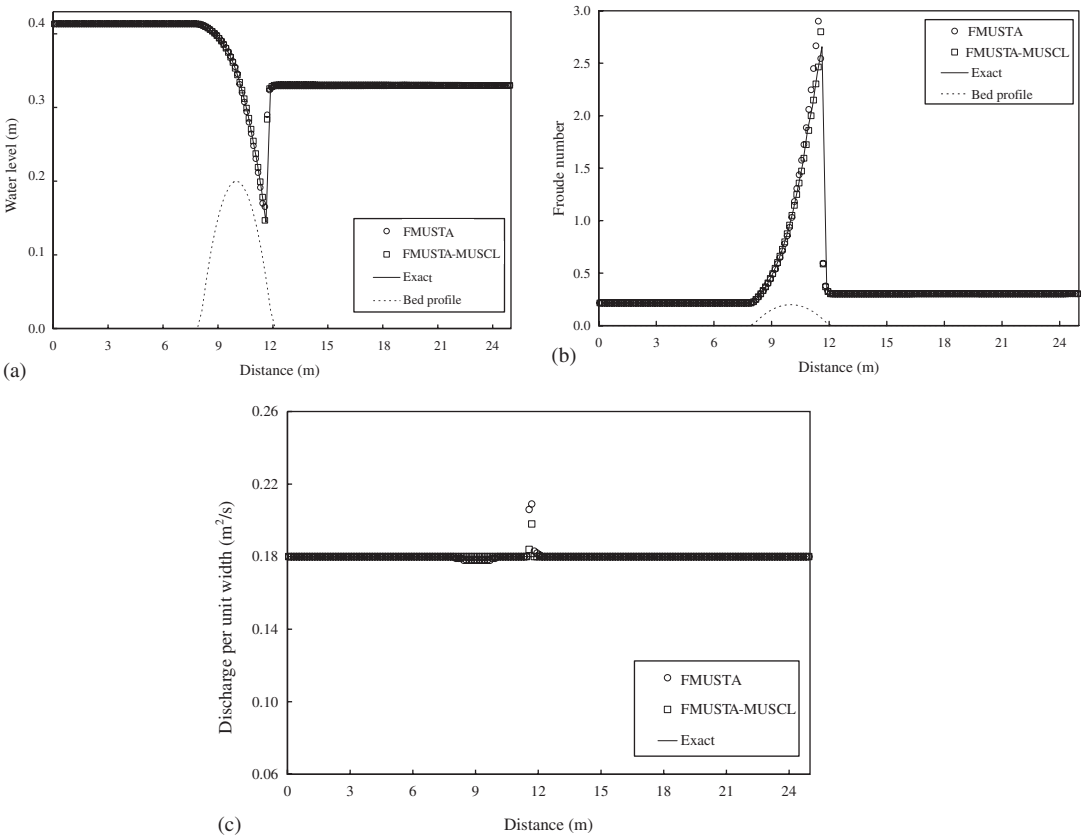

Figure 9. Comparison of the exact solution with the simulated (a) water levels, (b) Froude numbers and (c) discharge per unit width using the FMUSTA and FMUSTA-MUSCL schemes ($K=1$) for the steady transcritical test flow.

and discharges per unit width. Consequently, the satisfactory simulated results demonstrate the capability of the proposed schemes coupled with the SGM in dealing with bed slope variations.

4.3. 2D Oblique hydraulic jump

When a converging vertical wall is deflected along the channel contraction through an angle δ inwards the supercritical flow, as shown in Figure 10, an oblique hydraulic jump originating at point O is produced with an angle of β. The purpose of this commonly tested problem [10–12, 18, 27] is to verify the performance of the proposed schemes for predicting the steady supercritical flow with a hydraulic shock. The angle between the converging wall and the flow direction is given by $\delta=8.95°$. The initial supercritical flow conditions are given by the water depth of 1 m, the velocity component u of 8.57 m/s and v of zero, corresponding to a Froude number of 2.74. The supercritical inflow boundary conditions of $h=1\,\text{m}, u=8.57\,\text{m/s}$ and $v=0\,\text{m/s}$ are imposed at the upstream inflow boundary. At the downstream outflow boundary, the transmissive boundary conditions are given [8]. The computational time step is set to be 0.02 s. The computational mesh

DOI: 10.1002/fld

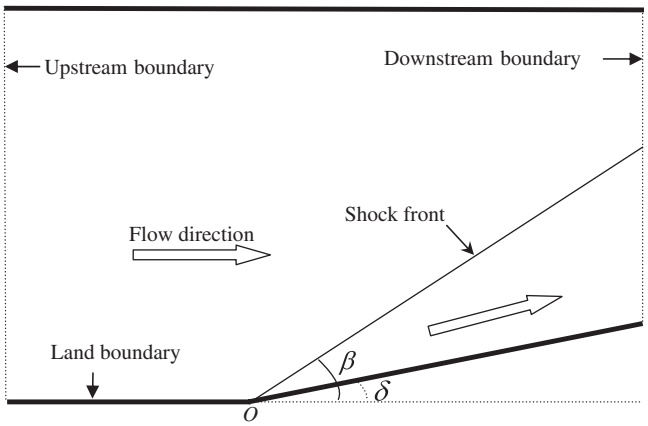

Figure 10. The 2D oblique hydraulic jump problem.

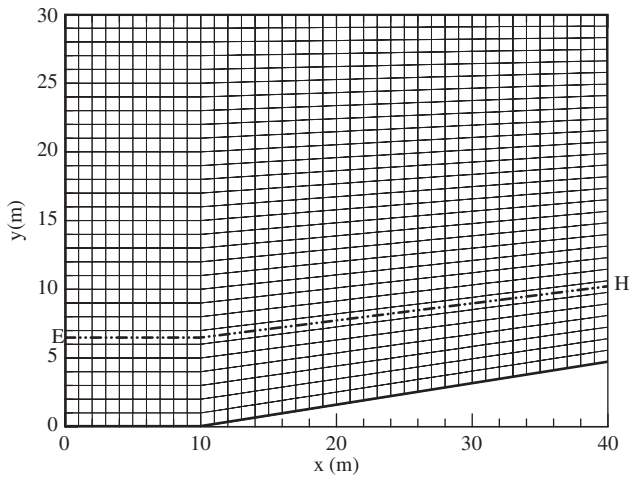

Figure 11. The computational mesh for the 2D oblique hydraulic jump problem.

with 40×30 non-rectangular cells is used and shown in Figure 11. To obtain a steady-state solution, a convergence criterion represented by R is used and has the form

$$R = \sqrt{\frac{\sum (h_{i,j}^{n+1} - h_{i,j}^{n})^2}{\sum (h_{i,j}^{n})^2}} \leqslant 1.0 \times 10^{-5} \tag{33}$$

where $h_{i,j}^{n}$ and $h_{i,j}^{n+1}$ are the computed water depths at the time steps n and $n+1$, respectively.

Figure 12 shows the simulated water depths using the first-order FMUSTA scheme along Line EH illustrated in Figure 11. The simulated results by the Roe and HLL schemes are plotted in Figure 12 for comparison. The comparison with the exact solution [30] shows that the proposed

DOI: 10.1002/fld

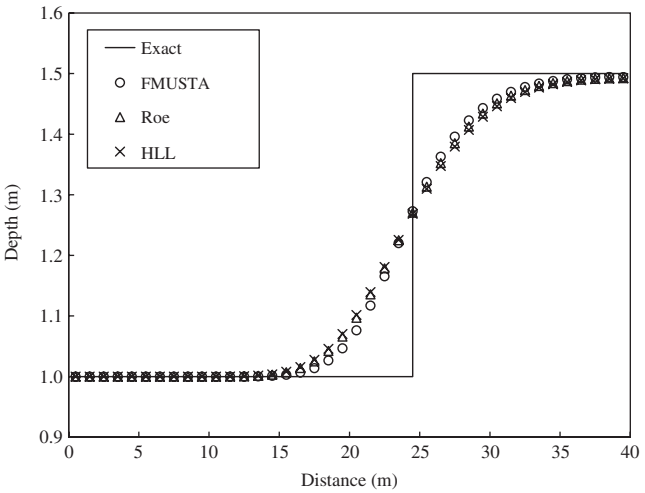

Figure 12. Comparisons of the exact solutions with the simulated water-depth profiles along Line EH (see Figure 11) using first-order schemes.

Table V. The error norms obtained from the first-order schemes for 2D oblique hydraulic jump problem.

Scheme	L_1	L_2	L_∞	CPU for convergence criterion (s)	Number of iteration
FMUSTA ($K=1$)	0.0182	0.0493	0.331	1.94	206
Roe	0.0208	0.0526	0.331	2.21	220
HLL	0.0214	0.0533	0.331	1.61	220

FMUSTA scheme resolves the jump without spurious oscillation and slightly sharper than the Roe and the HLL schemes. Table V lists error norms from the simulated results, including L_1, L_2 and L_∞. Besides, the CPU time for reaching the convergence criterion is summarized in Table V. It is found that all of the schemes obtain the same error norms of L_∞. The CPU time consumed by the Roe scheme is the largest among the schemes tested. The proposed FMUSTA scheme has a superior overall numerical accuracy according to the smallest error norms of L_1 and L_2.

Figures 13(a) and (b) show the contour plots of the simulated water depth by the FMUSTA and FMUSTA-MUSCL schemes, respectively. It is obvious that the second-order FMUSTA-MUSCL scheme achieves more accurate resolution than the first-order FMUSTA scheme.

4.4. Circular dam-break flow

The hypothetical test case studied by many researchers [7, 10–12] involves the breaking of a circular dam. This problem can be adopted to assess the capability of the proposed FMUSTA-MUSCL scheme in modeling 2D symmetric dam-break flow. The initial conditions include the two regions of still water separated by a cylindrical dam of radius 11 m. The initial water depth inside the dam is 10 m and outside is 1 m. A circular mesh with 50 cells in the tangential direction and 25 cells along the radial direction is employed herein. The computational time step is 0.02 s.

DOI: 10.1002/fld

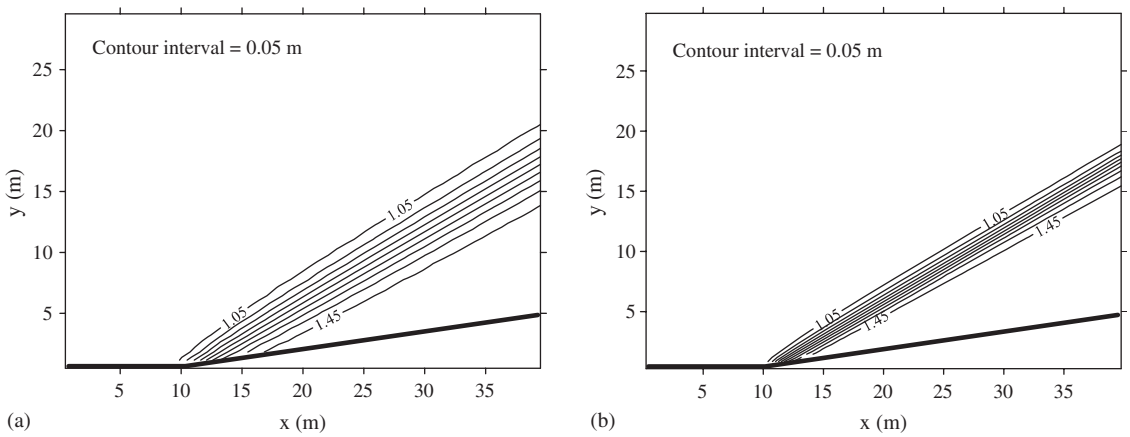

Figure 13. The contour plots of the 2D oblique hydraulic jump problem using (a) the FMUSTA and (b) FMUSTA-MUSCL schemes ($K=1$).

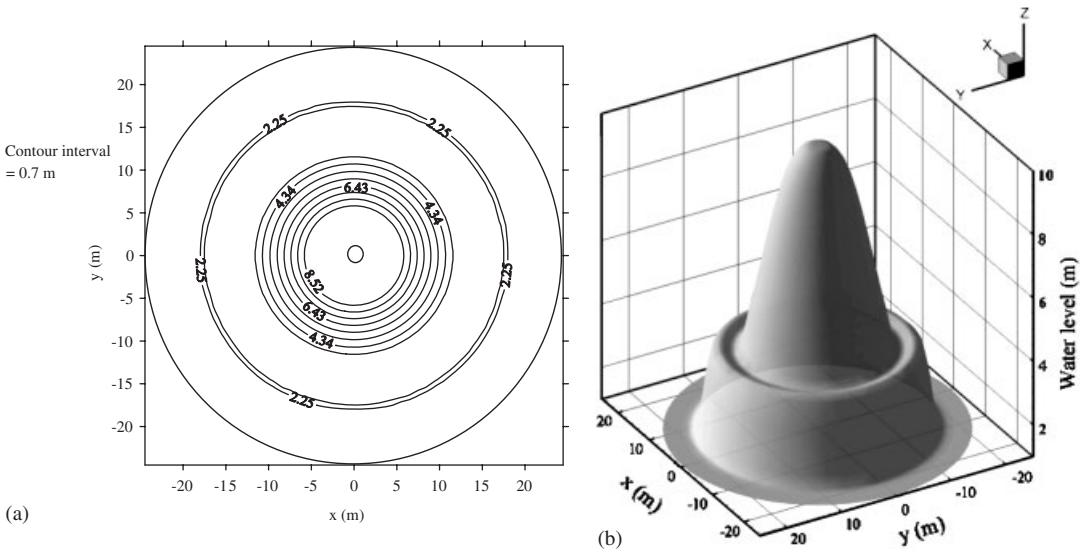

Figure 14. (a) The 2D contour plot and (b) 3D free-surface view showing water-depth variations for the circular dam breaking at $t=0.69$ s using the FMUSTA-MUSCL scheme ($K=1$).

The 2D contour as well as the 3D view of the water surface elevation at $t=0.69$ s simulated by the second-order FMUSTA-MUSCL scheme ($K=1$) are shown in Figures 14(a) and (b), respectively. Compared with the simulated results by the other schemes [7, 10–12], the proposed FMUSTA-MUSCL scheme produces the satisfactory results, in which there are clearly an outward-propagating circular shock wave and an inward-propagating circular rarefaction wave.

DOI: 10.1002/fld

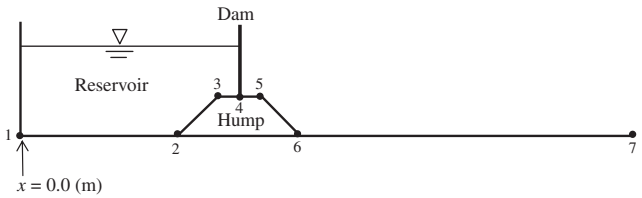

Point number	x (m)	Bed elevation (m)
1	0.00	0.0
2	2.00	0.0
3	2.20	0.108
4	2.25	0.108
5	2.30	0.108
6	2.50	0.0
7	7.00	0.0

Figure 15. The layout of the dam-break experiment with a hump.

4.5. Dam-break flow over a hump

To demonstrate the capability of the proposed FMUSTA and FMUSTA-MUSCL schemes for simulating dam-break flow with the abrupt bed variations, the dam-break flow over a hump with the experimental data is simulated. The dam-break experiment was reported by Aureli *et al*. [31] and conducted in a rectangular channel with a length of 7 m and width of 1 m. The detailed experimental domain, including the locations of the dam and hump, is shown in Figure 15. The initial upstream water level is 0.35 m and the downstream depth is 0 m, i.e. the dry-bed condition. To avoid mathematical difficulty in the dry-bed simulation, an almost negligible water depth of 0.00001 m is imposed at the downstream of the dam [8]. According to the calibrated value used in Aureli *et al*. [31], the Manning roughness coefficient is set to be 0.01. The land boundary conditions are imposed at the walls. At the upstream boundary, a zero-discharge condition is specified. At the downstream end of the channel, a transmissive boundary condition is imposed. The computational mesh with 144 uniform cells is employed. The computational time step is 0.01 s. The total simulation time is 15 s after dam break.

The comparisons between the measured data and the simulated water-depth hydrographs are shown in Figure 16. For all observation stations at $x = 1.4, 2.25, 3.4$ and 4.5 m, the simulated results including the shocks, the dry/wet fronts and the reverse flows agree closely with the measured. The numerical differences between the FMUSTA scheme and the FMUSTA-MUSCL scheme for all observation stations are almost the same. Both the proposed schemes do achieve very good resolutions in this dry-bed dam-break flow test case in the presence of abrupt bottom variations.

For comparison purposes, the generalized first-order centred (GFORCE) flux [15] is adopted in the MUSTA method to give the GMUSTA scheme and applied to the presented dam-break flow simulation. As an example, Figure 17 shows the comparison result at $x = 1.4$ m. The simulated results by using the upwind Roe and HLL schemes are also added for comparison. The simulated results show that all the presented schemes obtain global good agreement with the experimental data. The FMUSTA scheme consumes about 17% less CPU time than the GMUSTA scheme.

DOI: 10.1002/fld

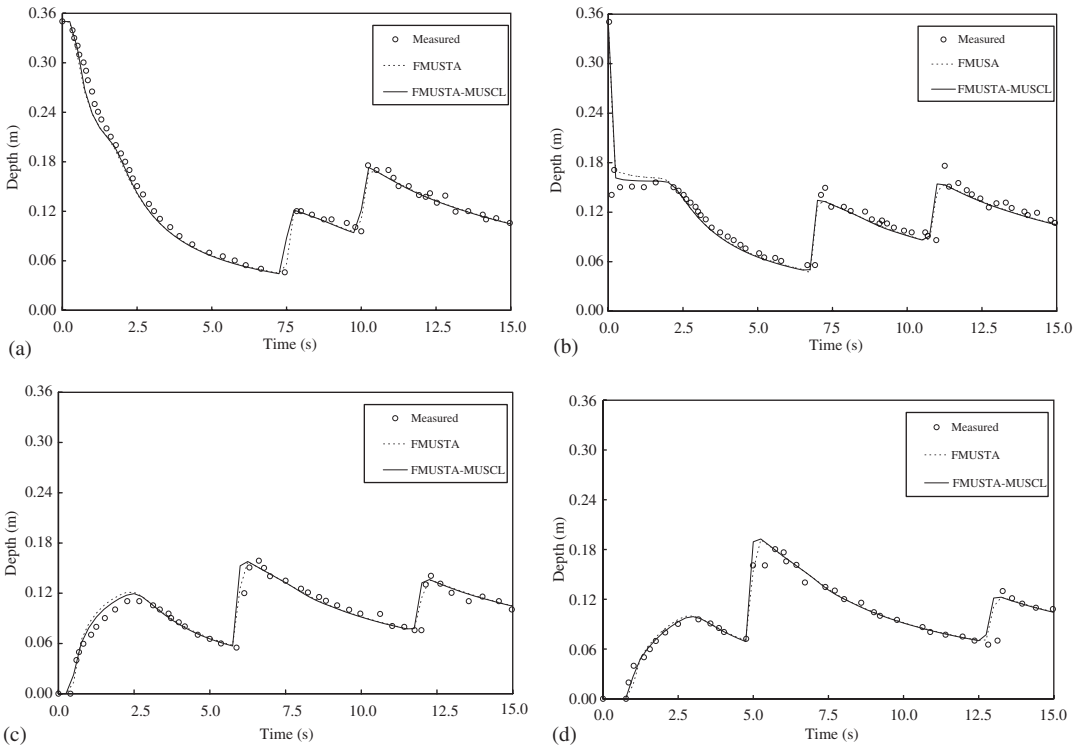

Figure 16. Comparisons of the measured and simulated results using the proposed schemes with $K=1$ at (a) $x=1.4$ m, (b) $x=2.25$ m, (c) $x=3.4$ m and (d) $x=4.5$ m for the dam-break flow over a hump.

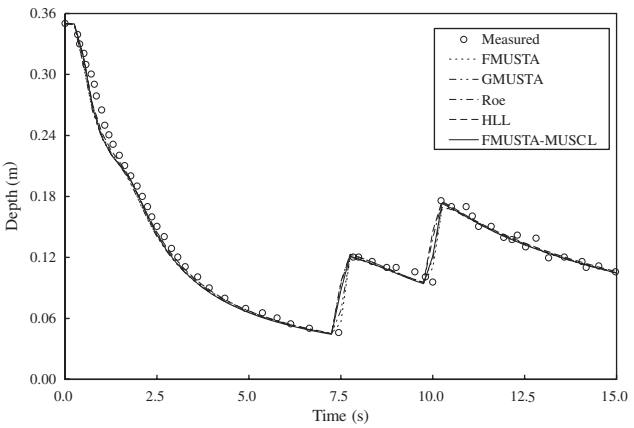

Figure 17. Comparison with other schemes at $x=1.4$ m for the dam-break flow over a hump.

DOI: 10.1002/fld

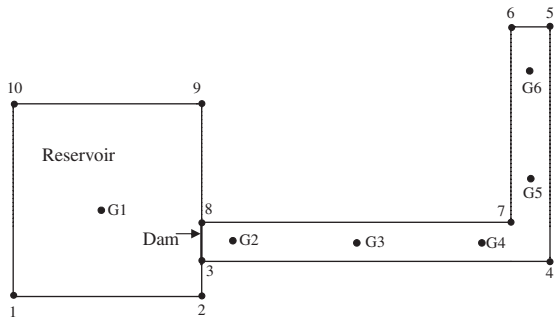

Point number	x (m)	y (m)	Observations	x (m)	y (m)
1	0.0	0.0	G1	1.19	1.20
2	2.39	0.0	G2	2.74	0.69
3	2.39	0.445	G3	4.24	0.69
4	6.805	0.445	G4	5.74	0.69
5	6.805	3.86	G5	6.56	1.51
6	6.31	3.86	G6	6.56	3.01
7	6.31	0.94			
8	2.39	0.94			
9	2.39	2.44			
10	0.0	2.44			

Figure 18. The layout of the dam-break experiment with the 90° bend channel.

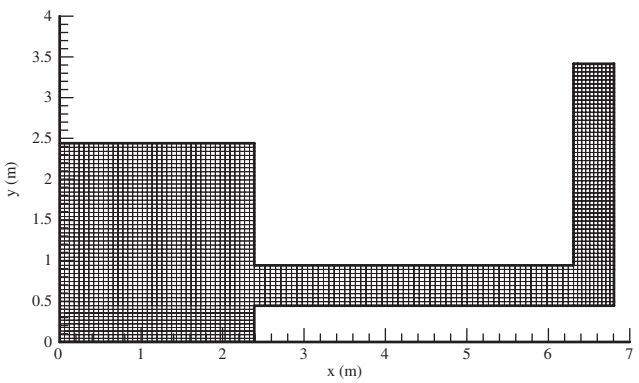

Figure 19. The computational mesh for the dam-break flow simulation with the 90° bend channel.

According to CPU-time consumption, the FMUSTA scheme would be a better choice for the practical shallow-water flow problems with the source terms.

4.6. Dam-break experiment with a 90° *bend channel*

The Concerted Action on Dam-Break Modeling project (CADAM) includes many dam-break experiments, which are useful benchmarks for numerical verifications [32]. The dam-break flow in

DOI: 10.1002/fld

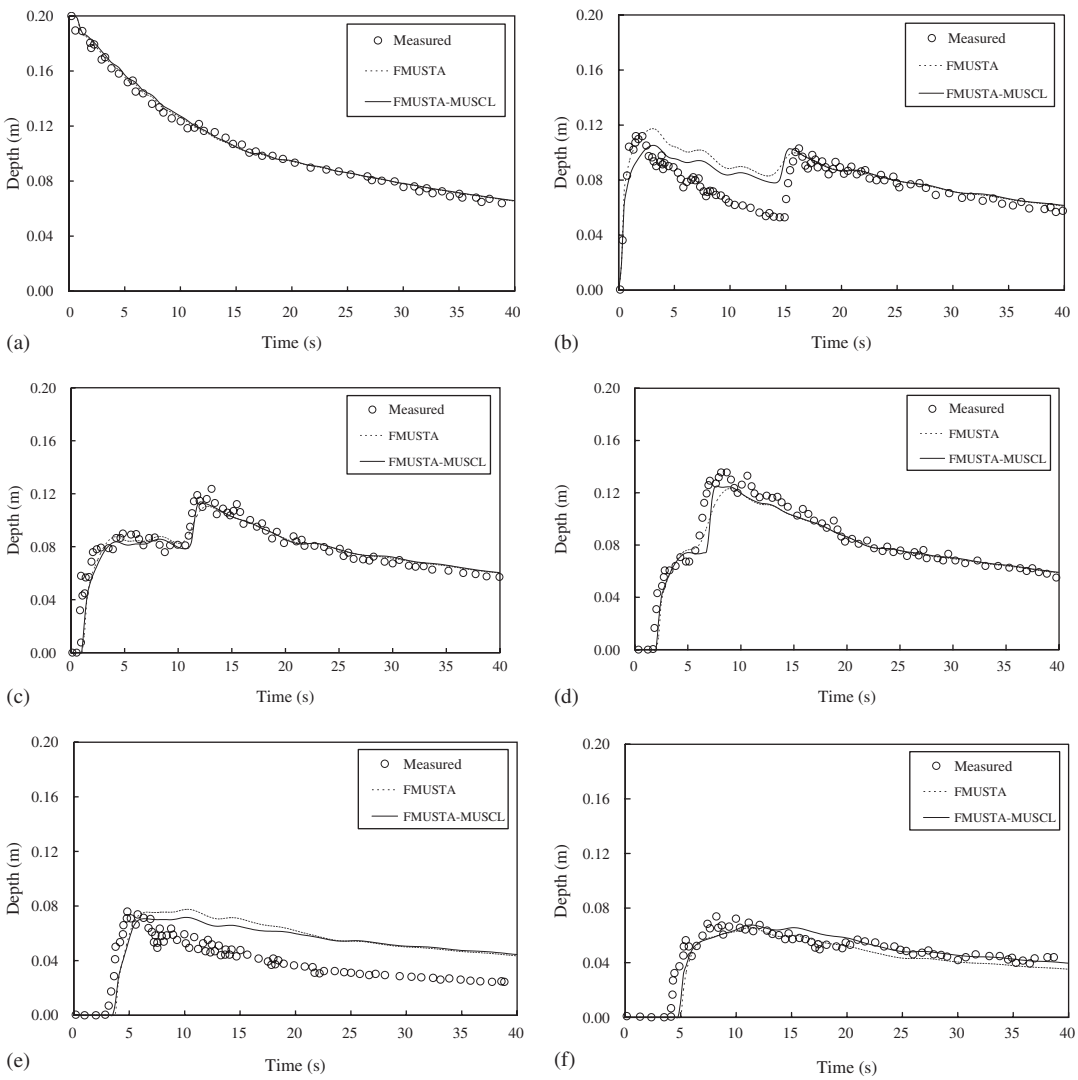

Figure 20. Comparisons of the measured and simulated water depths against time at Station (a) G1, (b) G2, (c) G3, (d) G4, (e) G5 and (f) G6 for the dam-break experiment with the 90° bend channel using the proposed schemes with $K = 1$.

a horizontal channel with a 90° bend is simulated herein. As shown in Figure 18, the experimental domain is a rectangular reservoir connecting to a channel with a 90° bend. The reservoir is separated from the channel by a dam. Then the dam is suddenly opened to produce a dam-break flow. Figure 18 also presents the geometry of the experiment and the locations of the observation stations. The initial water depths are 0.2 m in the reservoir and 0 m in the channel. The total simulation time is 40 s after dam break. The Manning roughness coefficient is calibrated to be 0.015. The

DOI: 10.1002/fld

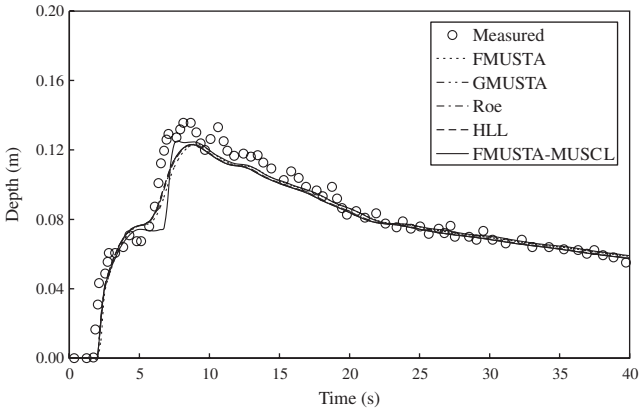

Figure 21. Comparison with other schemes at Station G4 for the dam-break experiment with the 90° bend channel.

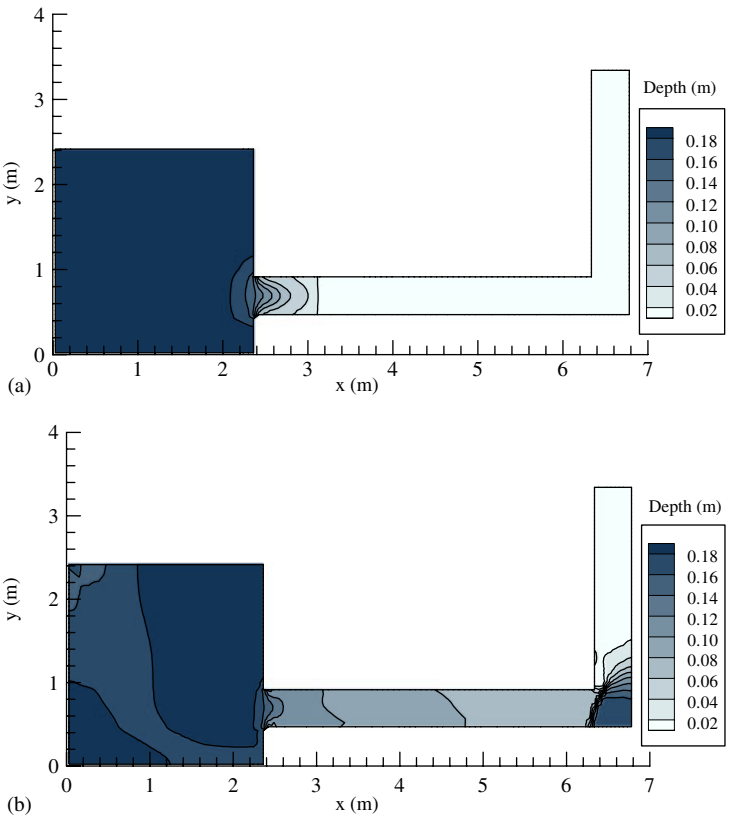

Figure 22. The simulated 2D contour plot showing water-depth variations for the dam-break experiment at: (a) $t=0.5$ s and (b) $t=4.0$ s by the FMUSTA-MUSCL scheme ($k=1$).

DOI: 10.1002/fld

computational mesh with 3200 non-rectangular cells, as illustrated in Figure 19, is used. The computational time step is 0.01 s.

Adopting the FMUSTA scheme and the FMUSTA-MUSCL scheme, the comparisons of the simulated water-depth hydrographs with the experimental data at different observation stations are shown in Figure 20. The results show the shock formation, propagation and reflection in the flow field. For all observation stations, the simulated water depths agree well with the measured. Apparently, the simulated results by the FMUSTA-MUSCL scheme are better than the FMUSTA scheme, especially for the G2 station. In addition, Figure 21 shows the simulation results at G4 as an example by the FMUSTA, GMUSAT, Roe, HLL and FMUSTA-MUSCL schemes for comparison. Small differences are observed between all tested first-order schemes. It implies that all first-order schemes give about the same solutions. This would have resulted by the inclusion of source terms in the shallow-water equations. However, the GMUSTA scheme is about 22% more expensive than the FMUSTA scheme. Comparing with the GMUSTA scheme, the attraction of the proposed FMUSTA scheme is its simplicity and efficiency. According to CPU-time consumption, the FMUSTA scheme would be a better choice for the practical shallow-water flow problems with the source terms.

By the FMUSTA-MUSCL scheme, the simulated 2D contour plots for water-depth variations at $t=0.5$ and 4.0 s are shown in Figures 22(a) and (b), respectively. According to the simulated results, the proposed schemes were found to be capable of resolving shocks, handling complex geometries with dry-bed condition.

5. CONCLUSIONS

For solving 2D SWE with source terms, the FVM and the multi-stage (MUSTA) method are employed to propose a finite-volume multi-stage (FMUSTA) scheme. The local Lax–Friedrichs numerical flux function is incorporated into the MUSTA method with FVM framework, leading to the first-order monotonic numerical flux. The predictor–corrector MUSCL method is employed to achieve the second-order accuracy in space and time. The SGM for the treatment of source terms is adopted to obtain the preservation of well-balancing property.

Adopting the proposed FMUSTA scheme requires the choice of the number of stages K in the local time marching. From the simulated results of the 1D idealized dam-break problems, the one-stage FMUSTA scheme ($K=1$) with two cells was found to be more efficient among the schemes tested in the present study and recommended for practical applications due to CPU-time consumption. On the basis of the calculated error norms and CPU-time consumption summarized in Tables I–III, the proposed FMUSTA schemes was found to be more accurate than the HLL scheme and more efficient than the Roe scheme. Compared with the popularly used Roe and HLL Riemann solvers, the proposed schemes do not require a detailed knowledge on the solution of the Riemann problem, leading to the ease coding and generality. Besides, the proposed schemes do not require the special treatment of entropy fixes and yet obtain high resolutions automatically for the class of dam-break problems with critical points at the dam site.

From the comparison of the exact solutions and the simulated results, the proposed schemes with the SGM do produce accurate solutions for the steady transcritical flow problem. On the basis of the 2D oblique hydraulic jump problem, the proposed FMUSTA scheme has superior overall numerical accuracy according to the smallest error norms of L_1 and L_2. Using the numerical test of the hypothetical (2D circular) dam-break flow problem, it is demonstrated that the proposed

DOI: 10.1002/fld

schemes have shock-capturing capability of the 2D circular propagating wave. The numerical verifications against the dam-break experiments demonstrate satisfactory capability and reliability of the proposed schemes in modeling the dry-bed dam-break flows with abrupt bed variations. It is concluded that the proposed schemes are accurate and efficient for modeling hydraulic shock waves in shallow-water flows.

ACKNOWLEDGEMENTS

The facilities provided for this study by the Hydrotech Research Institute, National Taiwan University, Taipei, Taiwan, are hereby gratefully acknowledged. Part of the financial supports from the National Science Council, Taiwan, under Grant Nos. NSC 95-2625-Z-002-022 and NSC 95-2622-E-002 -011-CC3 is highly appreciated.

REFERENCES

1. Roe PL. Approximate Riemann solvers, parameter vectors, and difference schemes. *Journal of Computational Physics* 1981; **43**:357–372.
2. Steger JL, Warming RF. Flux vector splitting of the inviscid gas dynamic equations with application to finite difference methods. *Journal of Computational Physics* 1981; **40**:263–293.
3. Osher S, Solomone F. Upwind difference schemes for hyperbolic systems of conservation laws. *Mathematics and Computers in Simulation* 1982; **38**:339–374.
4. Hirsch C. *Numerical Computation of Internal and External Flows*, vol. 2. Wiley: Chichester, 1990.
5. Toro EF. *Riemann Solvers and Numerical Methods for Fluid Dynamics*. Springer: Berlin, 1997.
6. LeVeque RJ. *Finite Volume Methods for Hyperbolic Problems*. Cambridge University Press: U.K., 2002.
7. Zoppou C, Roberts S. Catastrophic collapse of water supply reservoirs in urban areas. *Journal of Hydraulic Engineering* 1999; **125**(7):686–695.
8. Toro EF. *Shock-capturing Methods for Free-surface Shallow Water Flows*. Wiley: New York, 2001.
9. Wan Q, Wan H, Zhou C, Wu Y. Simulating the hydraulic characteristics of the lower Yellow River by the finite-volume technique. *Hydrological Processes* 2002; **16**(14):2767–2769.
10. Erduran KS, Kutija V, Hewett CJM. Performance of finite volume solutions to the shallow water equations with shock-capturing schemes. *International Journal for Numerical Methods in Fluids* 2002; **40**:1237–1273.
11. Lai JS, Lin GF, Guo WD. Simulation of hydraulic shock waves by hybrid flux-splitting schemes in finite volume method. *Journal of Mechanics* 2005; **21**(2):85–101.
12. Lai JS, Lin GF, Guo WD. An upstream flux-splitting finite-volume scheme for 2D shallow water equations. *International Journal for Numerical Methods in Fluids* 2005; **48**(10):1149–1174.
13. Toro EF. *Multi-stage Predictor–corrector Fluxes for Hyperbolic Equations*. Isaac Newton Institute for Mathematical Sciences Preprint Series. University of Cambridge: U.K., NI03037-NPA, 2003.
14. Titarev VA, Toro EF. MUSTA schemes for multi-dimensional hyperbolic systems: analysis and improvements. *International Journal for Numerical Methods in Fluids* 2005; **49**(2):117–147.
15. Toro EF, Titarev VA. MUSTA fluxes for systems of conservation laws. *Journal of Computational Physics* 2006; **216**:403–429.
16. Zhou JG, Causon DM, Mingham CG, Ingrams DM. The surface gradient method for the treatment of source terms in the shallow water equations. *Journal of Computational Physics* 2001; **168**:1–25.
17. Tan WY. *Shallow Water Hydrodynamics*. Elsevier: New York, 1992.
18. Lin GF, Lai JS, Guo WD. Finite-volume component-wise TVD schemes for 2D shallow water equations. *Advances in Water Resources* 2003; **26**(8):861–873.
19. Yu H, Liu YP. A second-order accurate, component-wise TVD scheme for nonlinear, hyperbolic conservation laws. *Journal of Computational Physics* 2001; **173**:1–16.
20. Leveque RJ. Balancing source terms and flux gradients in high-resolution Godunov methods: the quasi-steady wave-propagation algorithm. *Journal of Computational Physics* 1998; **146**:346–365.
21. Brufau P, Vazquez-Cendon ME, Garcia-Navarro P. A numerical model for the flooding and drying of irregular domains. *International Journal for Numerical Methods in Fluids* 2002; **39**:247–275.

DOI: 10.1002/fld

22. Zhou JG, Causon DM, Ingrams DM, Mingham CG. Numerical solutions of the shallow water equations with discontinuous bed topography. *International Journal for Numerical Methods in Fluids* 2002; **38**:769–788.
23. Brufau P, Garcia-Navarro P. Unsteady free surface flow simulation over complex topography with a multidimensional upwind technique. *Journal of Computational Physics* 2003; **186**:503–526.
24. Gallouet T, Herard JM, Seguin N. Some approximate Godunov schemes to compute shallow water equations with topography. *Computers and Fluids* 2003; **32**:479–513.
25. Audusse E, Bouchut F, Bristeau MO, Klein R, Perthame B. A fast and stable well-balanced scheme with hydrostatic reconstruction for shallow water flows. *SIAM Journal on Scientific Computing* 2004; **25**(6):2050–2065.
26. Wang JW, Liu RX. A comparative study of finite volume methods on unstructured meshes for simulation of 2D shallow water wave problems. *Mathematics and Computers in Simulation* 2000; **53**:171–184.
27. Guo WD, Lai JS, Lin GF. Hybrid flux-splitting finite-volume scheme for the shallow water flow simulations with source terms. *Journal of Mechanics* 2007; **23**(4):269–283.
28. Stoker JJ. *Water Waves*: *Mathematical Theory with Applications*. Wiley-Interscience: Singapore, 1958.
29. Alcrudo F, Benkhaldoun F. Exact solutions to the Riemann problem of the shallow water equations with a bottom step. *Computers and Fluids* 2001; **30**(6):643–671.
30. Hager WH, Schwalt M, Jimenez O, Chaudry MH. Supercritical flow near an abrupt wall deflection. *Journal of Hydraulic Research* 1994; **32**(1):103–118.
31. Aureli F, Mignosa P, Tomirotti M. Numerical simulation and experimental verification of dam-break flows with shocks. *Twelfth International Conference on Computational Methods in Water Resources*, Crete, Greece, 15–19 June 1998; 387–394.
32. Zhou JG, Causon DM, Mingham CG, Ingrams DM. Numerical prediction of dam-break flows in general geometries with complex bed topography. *Journal of Hydraulic Engineering* 2004; **130**(4):332–340.

DOI: 10.1002/fld